Journal of Visualization, Vol. 7, No. 1 (2004) 63-75

Phenomenon of Labyrinth Seal with Low Static Pressure Difference and Large Clearance

(Analysis of the Internal Phenomenon with CFD)

Shimada, K.*[1], Kimura, K.*[1], Ichikawa, S.*[1], Ohta, H.*[2] and Aoki, K.*[2]

*1 Product Development Center, Toyo Radiator Co., LTD. 4-14 Shioya-cho, Minami-ku, Nagoya, 457-8560, Japan.
*2 Department of Mechanical Engineering, School of Engineering, Tokai University, 1117 Kitakaname, Hiratsuka, Kanagawa 259-1292, Japan.

Received 26 September 2002
Revised 15 May 2003

Abstract : This paper discusses the straight-through type labyrinth seal. This labyrinth seal is used for axial flow fans, which have an outer ring at the blade tip to seal the clearance between the ring tip and the fan shroud, in order to prevent the reverse flow or leakage. These fans are used for the cooling of automobile radiators. In these cases, the labyrinth seal is used in an extremely low static pressure difference and a large clearance. A significant decrease of the leakage rate was reported even when the labyrinth seal rotated in comparatively low speed in this unique condition according to the authors' former report. However, this phenomenon is different from past research. Furthermore the cause of this phenomenon has not been determined. Therefore, the internal flow was depicted with Computational Fluid Dynamics (CFD) in order to clarify the cause of this phenomenon. The results of CFD show that the leakage rate decreases significantly because the carry-over flow is intercepted in the expansion groove. This is the newly discovered phenomenon which occurs under the unique condition of an extremely low differential pressure. It has not been pointed out before as the reason why the rotation decreases the leakage rate.

Keywords : Fan, Tip clearance, Labyrinth seal, Visualization, CFD

1. Introduction

In most cases, fans with an outer ring fixed at the blade tips are used for the axial flow fan in automobile radiators. The labyrinth mechanism of such fans whose ring is covered with a fan shroud reduces the leakage flow, and thus improves the fan's performance (Shimada et al., 2002). In this case, a labyrinth seal operates in an extremely low static pressure difference with a large clearance because of the low operating pressure of the radiator cooling fans and their imprecise structure made of plastic. The former report by the authors revealed a phenomenon that a leakage rate significantly decreased at a relatively low peripheral velocity when the labyrinth seal was rotated (Shimada et al., 2003). At this time, the leakage rate decreased by 44% at the peripheral velocity of the labyrinth seal, 49.7m/s, as compared with when the labyrinth seal was stationary. However, the past research that tested the correlation between the rotation of the labyrinth seal and the leakage rate (Komotori and Miyake, 1977) (Miyake and Ariga, 1987) reports that the decrease of the leakage rate is almost

nonexistent at the peripheral velocity of the labyrinth seal below 50m/s.

These past studies point out two causes that account for the decrease of the leakage rate when a straight-through type labyrinth seal rotates. Those are shown below as follows:

1. The increase of friction on the walls of the expansion grooves that is caused by a spiral flow.
2. The increase of diffusion of the inflow to the expansion grooves due to the seeming increase of relative fin pitches by the spiral flow mentioned above.

However, these causes are not verified by either measurement or visualization of the three-dimensional flow within the labyrinth seal, thus they remain mere hypothesis. In this way, the past studies have not completely revealed either the state of three-dimensional internal flow with the labyrinth seal rotating or the reasons for the decrease of the leakage rate due to its rotation.

The purpose of this report is to clarify the causes that lead to the significant decrease of the leakage rate, which differs from the results of the past studies. This report attempts to analyze the internal flow when the labyrinth seal rotates. Concretely, the performance tests of the labyrinth seal were conducted and make its characteristics clear. Next, the leakage flow rate which was led by Computational Fluid Dynamics (CFD) was compared with the test results and was verified. Then, it was allowed to depict the three-dimensional internal flow with CFD and then analyzed it. Furthermore, the visualization by a two-dimensional model was conducted and also the internal pressure in the actual model was measured, in order to investigate the CFD results of the internal flow and the internal pressure. As a result, an internal phenomenon which was not mentioned in the past research was newly observed. This phenomenon is the main cause of the significant decrease of the leakage rate by rotation, under the condition of an extremely low static pressure difference.

2. Experimental Method and Equipment

Figure 1 shows the equipment for the performance tests and the shape of the labyrinth seal. In the performance tests, the place for the fan is closed with a seal disc as shown in Fig.1(a). For the actual usage, an axial flow fan is set at the inside of the ring instead of the seal disc. No leakage occurs at the seal disc. Then it was attached to the fan testing chamber. The static pressure is applied to the upstream side, and the downstream side is exposed to open atmosphere when the leakage rate is measured under each condition. The operating static pressure difference of the fan in the automobile radiators is normally about 250Pa at maximum. Thus, the static pressure difference in the range of 50~250Pa is applied to the fan testing chamber so as to conduct the tests. In other words, test conditions of the static pressure difference must be identified with the operating static pressure difference of the radiator cooling fan, because the operating pressure of both the fan and the labyrinth seal must always agree. Also, the number of revolution for the radiator cooling fan is normally about 2500rpm at maximum. In this case, the peripheral velocity of the ring tip of the

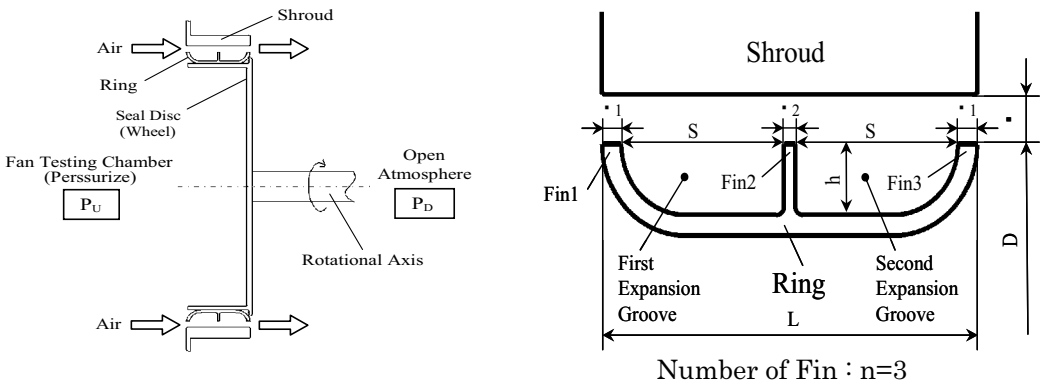

(a) Test rig (b) Specification of the ring (n=3)

Fig. 1. Configurations of the test rig and the Labyrinth seal.

labyrinth seal is U=47.4m/s. Thus, rotation was added to the ring in the range of U=0~47.4m/s in the performance tests.

Figure 1(b) shows the shape of the labyrinth seal (ring) used in this study. It has three fins and two expansion grooves in-between each fin. The clearance area forms a linear channel from the inlet through the outlet. Labyrinth seals such as these are generally called a straight-through type. Their structure is simple enough to be assembled easily so that they are widely used. Fin1 and Fin3 are bent and form a bell mouth in order to achieve an efficient intake of the air to the fan and discharge it from the fan. These fans which have a ring are mass-produced with glass fiber reinforced plastic by an injection molding machine. Therefore, the thickness of the ring is determined by the strength, weight and cost, also formability of resin. Fin2 is not concerned with the structural strength of the ring. Therefore, Fin2 is thinner than the other fins. Fin2 is located in the middle between Fin1 and Fin3 in order to halve an expansion groove formed with Fin1 and Fin3. The authors tested the performance of the labyrinth seals by ueing different numbers of fins. The labyrinth seal which has three fins, shown in Fig.1, achieved the highest performance (Shimada et al., 2003). Therefore this labyrinth seal is used as a research subject in this study. The height of each fin in the radial direction is constant throughout at h=8.5mm, while the diameter of the fin tip (ring tip) is constant throughout at D=362mm. The clearance between the inner wall of the cylindrical shroud and the tips of the fins is ε=3mm. Here, the entire length of the ring is L=49.7mm and each space between the fins is S=21.6mm. The thickness of each fin at the inlet and the outlet is $\delta 1$=2.5mm and that of the fin in the center is $\delta 2$=1.5mm. In addition, the arc shape of the ring is identical at the inlet and the outlet.

3. Results of Performance Tests

Figure 2 shows the test results of the leakage rate at the labyrinth seal. The ordinate shows a labyrinth function Φ, while the abscissa shows the static pressure difference in the chamber Ps and its dimensionless number $1-\lambda$. λ is the pressure ratio which is expressed as $\lambda = P_D/P_U$. P_D is the absolute static pressure at the outlet of the labyrinth seal. P_U is the absolute static pressure at the inlet of the labyrinth seal. The range of Ps in the abscissa is the same as the rage of operating pressure of the cooling fan, and that is from 50Pa to 250Pa. The labyrinth function is the flow rate function that corresponds to the dimensionless parameter of the leakage rate. Equation (1) is predominantly used to represent the labyrinth function, where G_E : the leakage rate of the labyrinth seal (kg/s), F : the sectional area of the clearance (m^2), ν_U : the specific volume of air at the inlet of the labyrinth seal (m^3/kg). Also, U : the peripheral velocity at the ring tip (m/s). Figure 2 demonstrates that the leakage rate increases with an increase in the static pressure difference Ps at each U. However, the leakage rate decreases with an increase in U. The tendency of this phenomenon is especially obvious in the region of low static pressure difference.

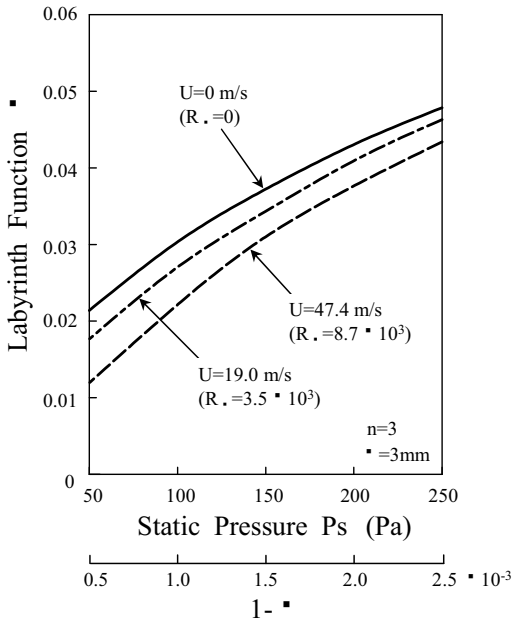

Fig. 2. Effect of rotation with different ring speed.

$$\Phi = G_E \left(F \sqrt{\frac{P_U}{\nu_U}} \right)^{-1} \tag{1}$$

Figure 3 shows changes in the leakage rate with the specific leakage rate Γ when the peripheral velocity U was given to the ring. Γ is the ratio of the leakage rate with the rotation G_{Er}, to the leakage rate without the rotation G_{Es}, and is represented with $\Gamma=G_{Er}/G_{Es}$. When the static pressure difference is set at Ps=250Pa, Γ decreases with an increase in U, and it reaches Γ=0.9 at U=47.4m/s. Thus, there is a 10% decrease in the leakage rate, as compared to that without the rotation. The tendency of that phenomenon is especially obvious when the static pressure difference is set as low as Ps=50Pa, then Γ reaches Γ=0.56 at U=47.4m/s. This finding differs significantly from the test results by Komotori (Komotori and Miyake, 1977), which was conducted under a high static pressure difference with a small clearance.

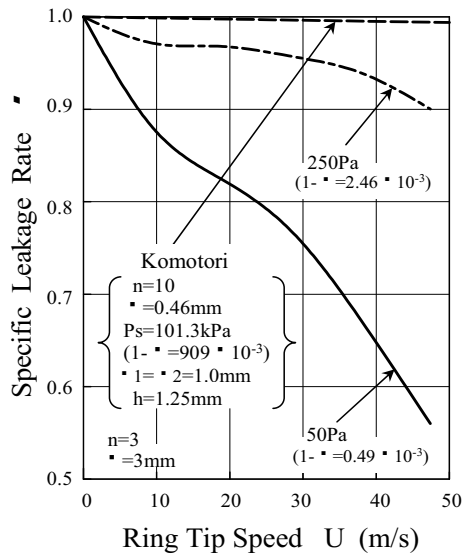

Fig. 3. Effect of rotation with different static pressure.

4. Analysis of Internal Flow of Rotating Ring with CFD

4.1 Conditions of CFD and Verifications of CFD Results

In order to clarify the reasons for the occurrence of the phenomenon in the previous chapter, the three-dimensional analysis of the internal flow was performed by using CFD. For executing computation, the Renormalization Group (RNG) k-ε turbulence model which is suitable to solve the problems of flow accompanied by separating or circulating flow is employed. In this computation, the versatile thermal fluid analysis software STAR-CD Version 3.10B was used. (Computational Dynamics Limited, 1999)

Figure 4 shows the configuration of the computational model, the boundary conditions and a detail of the grids condition around the inlet. This model is a full-scale and the operating fluid is standard air. Therefore, a specified Reynolds number is not given for this computation. The figure of a whole computational model has formed a wedge which has a section to solve the flow problems to apply cyclic boundaries. Here, the wedge angle is 5 degrees. The cyclic boundaries consist of pairs of geometrically identical boundaries at which the flow repeats itself. Therefore, this property can be exploited to reduce the size of the computational domain and associated computing overhead. It is predicted that the flow in the labyrinth seal is identical in all axial plains containing the symmetry axis. Consequently, it is possible to apply these boundaries to solve the internal flow of the labyrinth seal. However, the static pressure boundaries are prescribed in order to identify that computational condition with the actual performance tests which are conducted to boost the fan testing chamber. The plains which are applied to these boundaries are located at 400mm upstream and at 1000mm downstream from the inlet and the outlet of the labyrinth. The location of the static pressure boundary in the upstream side is identical to the location of measuring holes for the static pressure in the fan testing chamber. In addition, rotational condition was applied for the surface of the ring and the seal disc.

The total number of the computational grid is approximately 3.1×10^5. The highest density of the computational grids was applied inside of the ring because the complicated flow that accompanies eddies and separation is expected here. The operating static pressure difference is 250Pa at maximum and the peripheral velocity of the ring tip is 37.9m/s at maximum in this computation. In this case, the maximum Mach number of the internal air flow is able to be estimated around 0.1. Consequently, this computation was conducted on the assumption of incompressibility. The calculation focuses on grasping the outline of the dominant internal flow so that it is done in a steady-state. A sufficient buffer region in the computation is set at the downstream sides in order to

prevent the stream which already left the outlet from affecting the computational results.

The leakage rates obtained from the computation were compared with that of the test results shown in Chapter 3. As well, the visualizing experiment in a two-dimensional model was conducted through a surface floating tracer method in order to investigate the computation results of the flow vector when the ring is stationary. In the process of the visualization, minute aluminum particles are let uniformly afloat on the water surface and their traces are photographed with slow shutter speed. At this time, the Reynolds number is equaled with the actual case, and is about 5.0×10^4 when the representative length of the number is applied as the length of the ring. In addition, the static pressure on the inner wall of the cylindrical shroud is measured with the actual device in order to investigate the computation results of the static pressure. A static pressure hole for the measurement, whose diameter is 0.5mm, is made vertically on the inner wall of the shroud at its center. Four more holes of the same size are made on both sides of the center hole in the axial direction at a regular pitch of 4.6mm. Therefore, nine holes in total are made in the axial direction. The tests are conducted at Ps=50Pa when U is 0m/s and 37.9m/s, respectively. This allows the investigation of the computation results for the static pressure distribution on the inner wall of the shroud both with and without the rotation.

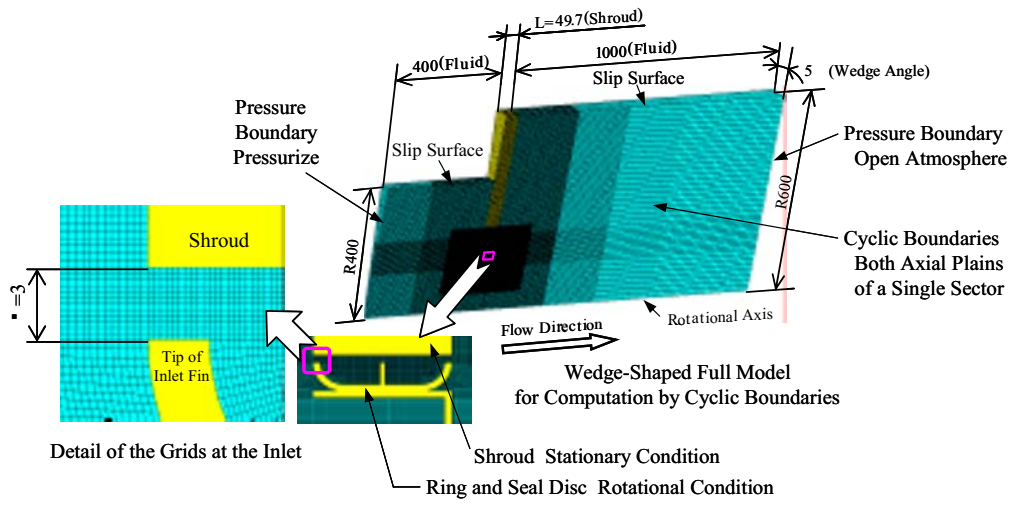

Fig. 4. Structure of computational model with boundary conditions and grid density at Inlet.

4.2 Results of CFD and its Verifications when Ps=250 Pa

Figure 5 shows the comparison of the values from the performance tests and the computation results at Ps=250Pa. The abscissa shows the rotational Reynolds number R_ω which is the dimensionless parameter of the ring tip peripheral velocity U. The ordinate shows the labyrinth function Φ. Here, R_ω is represented as in equation (2).

$$R_\omega = \frac{r_m \omega \varepsilon}{\nu} \tag{2}$$

r_m is the mean radius which is represented as $r_m = (D+\varepsilon)/2$. ω is the angular velocity of the rotating ring. ν is the kinematic viscosity of the air. ε is the clearance. The computed values show an accuracy of 90~97% against the values from the performance tests. Φ gradually decreases with an increase in R_ω, and this tendency correlates with that of the test results. Thus, the computation results closely represent the influences of the rotation on the leakage rate.

Figure 7 shows the computation results of the internal flow without the ring rotation. The vectors here represent the resultant velocity of the axial and radial velocity components. The flow with high flow velocity passes straight through the clearance from the inlet to the outlet without an

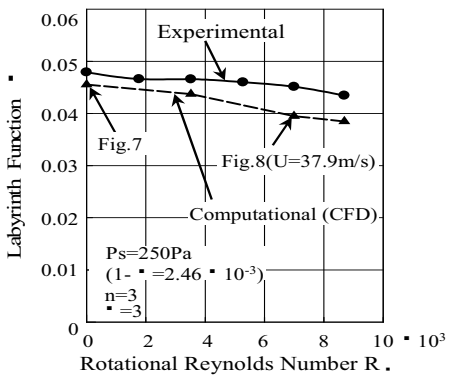

Fig. 5. Calibration of CFD for the effect of rotation when Ps=250Pa.

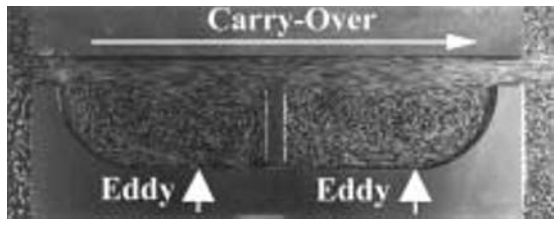

Fig. 6. Two-dimensional internal flow of the Labyrinth seal by surface floating tracer method.

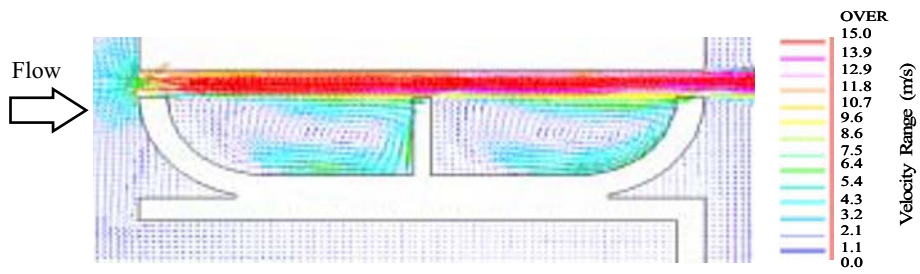

Fig. 7. Resultant velocity of the axial and radial components when the ring is stationary (R_ω=0).

expansion that sufficiently decelerates in the expansion grooves. Such a phenomenon is called a carry-over. Also, a large eddy is formed along the walls in each expansion groove. This state of the flow is as same as that shown in the visualization of Fig. 6 by the surface floating tracer method. Consequently, it can be said that the computation results almost accurately represent the actual internal flow when the ring is stationary. The tendency of the leakage rate of the computation results shown in Fig. 5 complies with the results of the performance test. Furthermore, the computation results of the internal flow without the rotation in Fig. 7 comply with the experimental result of visualization. Therefore, it is also deemed possible to analyze such fundamental phenomenon of the internal flow when the rotation was added.

Figure 8 shows the computation results of the internal flow when a peripheral velocity of U=37.9m/s ($R_\omega=7.0\times10^3$) is given to the ring. Figure 8(a) shows a vector map of the resultant velocity of the axial and radial velocity components. In comparison with the case of the stationary ring rotation, there is no significant difference. However, centrifugal force that works on the walls of each fin vacuums the air in the radial direction. As a result, stagnation areas at the root of Fin1 and Fin2 on the downstream side disappear. Thus, the eddies in the expansion grooves develop. Also, carry-over decreases and the flow velocity at the clearance decreases slightly. Figure 8(b) shows the contour map of a peripheral velocity component. On the surface of the ring that includes the seal disc, a high peripheral velocity arises due to viscous friction between the rotating ring and the air. In Fig. 8(a), the flow collides into the fin's walls on the upstream side and the flow velocity increases in this part. In Fig. 8(b), the peripheral velocity begins to be accelerated from this part along the rotational direction of an eddy in the grooves. This peripheral velocity merges with the carry-over flow whose velocity is high, at the fin tips. Then, the peripheral velocity gradually loses velocity as it is flowed downstream from the fin tips. In other words, there is a cycle that a little slow flow from the carry-over into the expansion grooves and is accelerated significantly in the peripheral direction on the wall of the expansion grooves, then the high velocity decreases again as it merges with the

carry-over at the clearance. The carry-over at the clearance is dominated by the axial velocity, thus the velocity component in the peripheral direction is relatively small. Conversely, the peripheral velocity dominates in the expansion grooves.

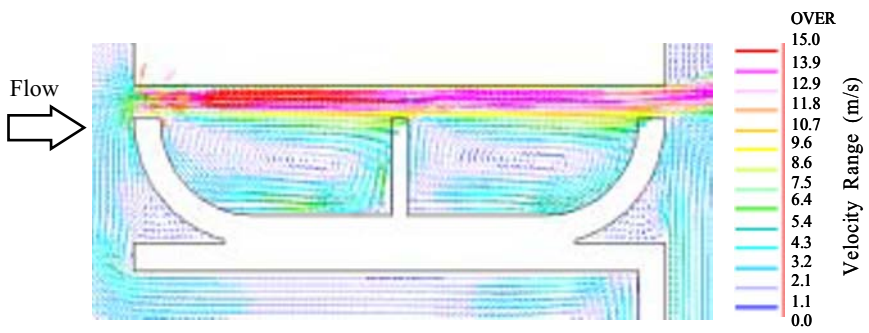

(a) Resultant velocity of the axial and radial components when the ring speed U=37.9m/s (R_ω=7.0×10^3)

(b) Peripheral velocity when the ring speed U=37.9m/s (R_ω=7.0×10^3)

Fig. 8. Visualization with CFD when the pressure condition Ps =250Pa (1-λ=2.46×10^{-3}).

The following section discusses the reasons for the decrease of the leakage rate due to the rotation. At Ps=250Pa and U=37.9m/s (R_ω=7.0×10^3), as shown in Fig. 3, the leakage rate decreases by approximately 7% in comparison to the case without the rotation. The result still makes a significant difference when compared with the results of Komotori, even though the percentage is smaller in comparison with the case at Ps=50Pa. In this case, the velocity component in the peripheral direction is very small in the carry-over at the clearance even though it is a main leakage flow, as shown in Fig. 8(b). Therefore, neither the first nor the second item of the existing reasons for the decrease of the leakage rate by rotation, which were stated in chapter 1, can be applied for this case. When considering the first item, the large friction loss of the main leakage flow by the high peripheral velocity on the wall of the labyrinth seal does not occur from the rotation. When considering the second item, the enlargement of the seemingly relative fin pitches, which is the view from the flow at clearance, does not occur from the rotation. Meanwhile, the leakage rate in Komotori's results shown in Fig. 3 only decreases slightly as well. Therefore, the past studies cannot reveal a main cause of the leakage rate decrease in this case.

4.3 Results of CFD and its Verifications when Ps=50 Pa

Figure 9 shows the comparison of values from the performance tests at Ps=50Pa and the computation results. The computed values show an accuracy of 87~96% against the values from the performance tests. Also, Φ of the computation results gradually decreases with an increase in R_ω and complies with the tendency of the test results. Thus, the computation results closely represent the influence of the rotation on the leakage rate. Figure 10 shows the computation results of the internal flow without the rotation. Vectors here represent the resultant velocity of the axial and radial velocity components. A carry-over with high flow velocity is observed at the clearance. Also, a

large eddy is formed along the walls in each expansion groove and stagnation areas with low flow velocity are observed at the root of the fins on their downstream side. The visualizing experiment through the surface floating tracer method shown in Fig.6 does not show the presence of such large stagnation areas. This is due to the Reynolds number used for the visualization that is set high when Ps=250Pa. Therefore, in the case at Ps=50Pa, as shown in Fig. 10, the flow velocity of the eddies in the expansion grooves is so slow that they do not have sufficient energy to reach the fin in the front. This is the reason why those large stagnation areas exist. In other words, this is one of the predicted conditions of the flow. The tendency of Φ through the computation shown in Fig. 9 complies with the results of performance test as mentioned above. Furthermore, the computation result of the internal flow without the rotation in Fig. 10 complies with the experimental result of visualization. Therefore, it is also deemed possible to analyze such fundamental phenomenon of the internal flow when the rotation was added.

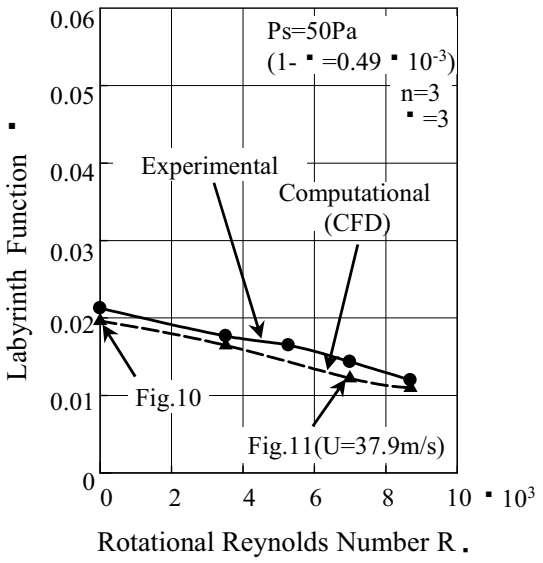

Fig. 9. Calibration of CFD for the effect of rotation when Ps=50Pa.

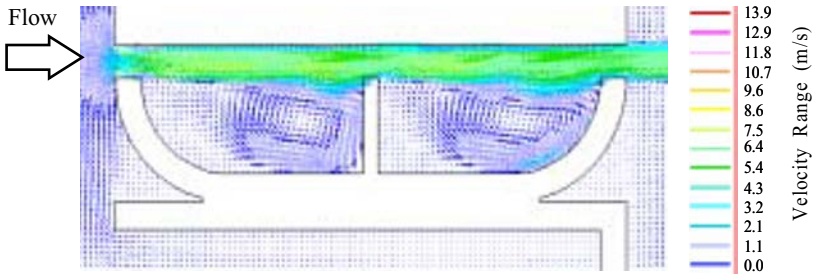

Fig. 10. Resultant velocity of the axial and radial components when the ring is stationary (R_ω=0).

Figure 11 shows the computation results of the internal flow when the peripheral velocity U=37.9m/s ($R_\omega=7.0\times10^3$) was given. Figure 11(a) shows a vector map of the resultant velocity of the axial and radial velocity components. There is a significant difference in the internal flow when compared to the case without the ring rotation shown in Fig. 10. The flow at the clearance that jets out at the fin tips does not pass through to the next fin. It separates from the shroud wall and it is bent toward the inside of the expansion grooves. This flow diffuses within the expansion grooves and some of it forms an eddy and some of it flows toward the outlet while changing its direction. In other words, the carry-over is cut off even though it passes through in a straight-through type labyrinth seal that forms a straight flow path at a large clearance. As is shown in Fig. 3, the leakage rate decreases by 33% in comparison to the case without the rotation, under the conditions of Ps=50Pa and U=37.9m/s shown in Fig. 11. Consequently, it has been found that this drastic decrease of the leakage rate is mainly due to the cut-off of the carry-over flow at the clearance mentioned above, from the result of this computation. There is no precedence in the past research that points out such a phenomenon as the reason for the leakage rate decrease in a straight-through type labyrinth seal when it is rotating. Figure 11(b) shows a contour map of a peripheral velocity component. What characterizes it is that the flow with very little peripheral velocity penetrates deeply into the expansion grooves. Figure 11(a) demonstrates that the flow at the clearance changes its direction

toward the inside of the expansion grooves. Therefore, the peripheral velocity within the expansion grooves is relatively low and the area with high peripheral velocity is limited to the wall surface area of the expansion grooves.

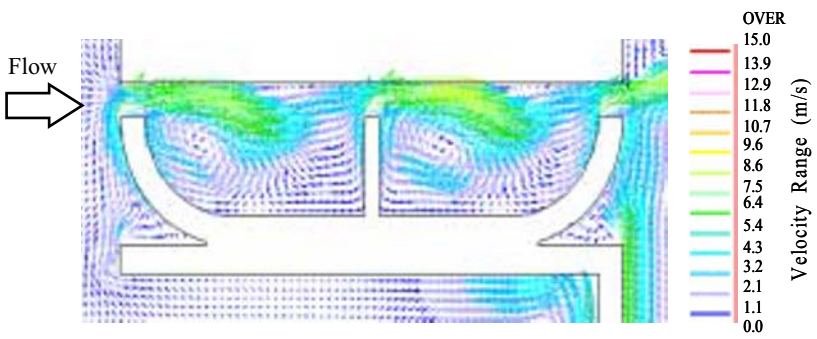

(a) Resultant velocity of the axial and radial components when the ring speed U=37.9m/s (R_ω=7.0×10^3).

(b) Peripheral velocity when the ring speed U=37.9m/s (R_ω=7.0×10^3).

Fig. 11. Visualization with CFD when the pressure condition Ps =50Pa（1-λ=0.49×10^{-3}).

The following section discusses the reasons for the changes of the direction of the carry-over flow into the expansion grooves or the cut-off of the carry-over flow. Two principal and possible reasons are predicted for this phenomenon. The first one is the static pressure differentials in the radial direction in the expansion grooves. The second one is that some viscous force exerted on the carry-over flow. First, the influences of the static pressure differentials are discussed with Fig. 12. Figure 12(a) shows the static pressure distribution when the ring is stationary. The static pressure becomes lower toward the downstream side. At this time, it is recognized that the static pressure on the walls and the tips of Fin2 and Fin3 on their upstream side is high. The reason is that the high velocity flow at the clearance diffuses and collides into the wall and also grazes the fin tips. Figure 12(b) shows the static pressure distribution when U=37.9m/s (R_ω=7.0×10^3). The static pressure on the walls of Fin2 and Fin3 on their upstream side is similarly high as in the case shown Fig. 12(a). However, its absolute value is much higher. The reason is that the high velocity flow of carry-over changes its direction toward the expansion grooves and their walls. In addition, the static pressure within the expansion grooves is lower at the center of the eddies. The eddies are represented in Fig. 11(a). The static pressure around the eddies' center is higher. At this time, almost no static pressure differentials in the radial direction are observed in the grooves in Fig. 12(b), even though comparatively large differentials of the static pressure are observed in the axial direction. Therefore, it is not likely that the pressure differentials in the radial direction in the expansion grooves draw the carry-over at the clearance toward the expansion grooves. Thus, the first one of the two possible reasons mentioned above is not correct.

Static pressure on the inner wall of the shroud was measured with the actual device in order to

investigate these computation results of Fig. 12. Figure 13 shows the comparison of the computation results by CFD and the measured values from the tests. Figure 13(a) shows the case of Fig. 12(a). The static pressure shows a tendency to gradually decrease from the inlet toward the outlet. Even though the computation result of Fig. 13(a) shows higher absolute pressure than the test values, the tendencies of both results almost fit each other. Figure 13(b) shows the case of Fig. 12(b). The static pressure is high at the inlet and it decreases in the first expansion groove. However, it increases again, reaching its maximum value right in front of the central fin. Then the static pressure decreases substantially in the second expansion groove after going through the central fin.

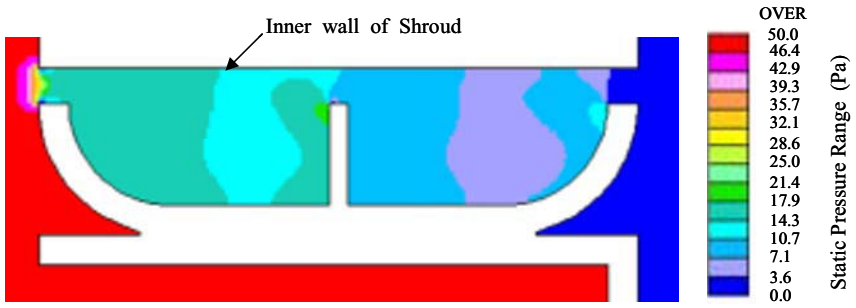

(a) Pressure contour when the ring is stationary (R_ω=0)

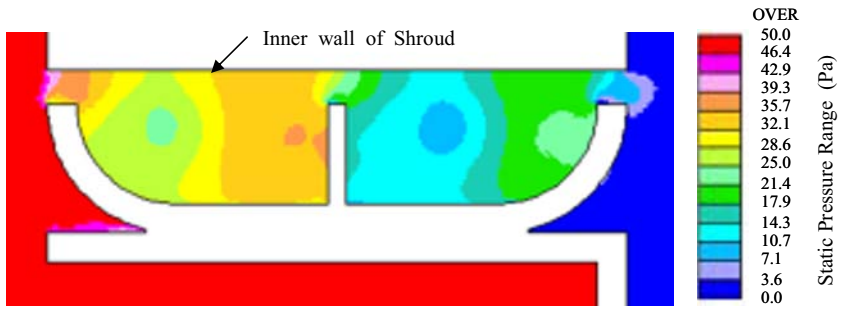

(b) Pressure contour when the ring speed U=37.9 m/s (R_ω=7.0×10^3)

Fig. 12. Contour map of static pressure when the pressure condition Ps=50Pa (1-λ=0.49×10^{-3}).

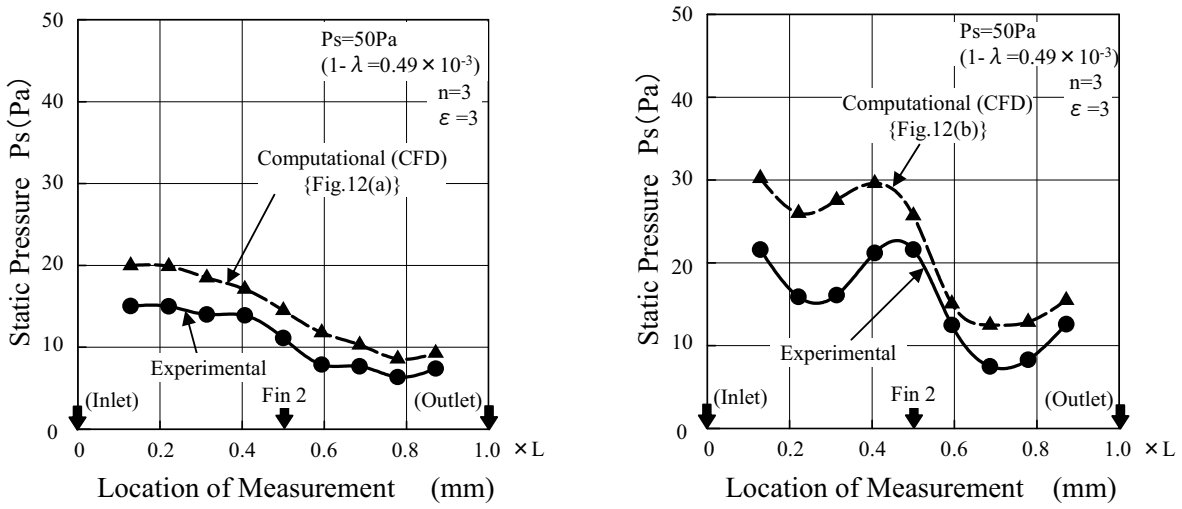

(a) When the Ring is Stationary (R_ω=0) (b) When the Ring Speed U=37.9 m/s (R_ω=7.0×10^3)

Fig. 13. Static pressure on the Inner wall of shroud when the pressure condition Ps=50Pa (1-λ=0.49×10^{-3}).

Afterwards, it reaches its minimum value around 0.7×L and increases again toward the outlet fin. The computation results of Fig. 13(b) likewise show higher absolute pressure than the test values, but the tendencies of both almost fit each other. Further evidence is that the location of the static pressure troughs around 0.23×L and 0.7×L in Fig.13(b) almost agree with the location of the eddy centers in the axial direction according to Fig. 11(a) and Fig. 12(b). It seems that the agreement proves the computation results in the respect of existence of the eddies and their location. Consequently, the computation results of the internal pressure both with and without the ring rotation fundamentally grasp the actual phenomenon. Also, this is the proof for the cut-off phenomenon of the carry-over shown in Fig. 11(a).

The influences of viscous force, will now be discussed. As mentioned previously, the flow within the rotating ring can be divided into circulating eddies in the expansion grooves and the peripheral flow on the wall of the expansion grooves. Thus, there is a possibility for either of them or for both of them participate in the cut-off phenomenon with the viscous force. First, circulating eddies are examined. As shown in Fig. 8(a), the circulating eddies are accelerated by centrifugal force on the fin's walls in the radial direction. However, that does not accelerate the eddies as a whole to increase their speed significantly. Thus, it is not likely that the accelerated eddies separate the carry-over flow from the shroud wall at the clearance due to their viscosity such that the flow is drawn into the expansion grooves. In order to confirm that, the computation of the internal flow was conducted under the conditions that the differential pressure between the inlet and the outlet is Ps=0, that there is no movement of the air in the axial direction, and that peripheral velocity U=37.9m/s (R_ω=7.0 $\times 10^3$) is given to the ring. Figure 14 shows the computation results. Figure 14(a) shows a vector map of the resultant velocity of the axial and radial velocity components. The flow in the radial direction arises in the areas of each fin tip, supposedly due to centrifugal force, and that forms two symmetrical eddies in each expansion groove. However, their flow velocity is about 2~3m/s on the surface of the fin tips, which is much slower in comparison with the flow velocity of the carry-over at the clearance. In other words, the flow velocity within the labyrinth that results from centrifugal force is very low. Therefore, the eddies that the ring rotation creates in the expansion grooves have little influence on the carry-over flow. Next, examined is the flow with high flow velocity in the peripheral direction on the wall of the expansion grooves. Figure 14(b) shows a contour map of a velocity component in the peripheral direction. Flow with high peripheral velocity arises in the areas of the expansion groove walls. In other words, the flow that the ring rotation causes is more dominant in the peripheral direction than in the radial direction. Likewise in the results shown in Fig. 8(b) as well as in Fig. 11(b), the peripheral flow velocity on the expansion groove wall is higher than 15m/s and this velocity is much higher than that of the eddies.

Studied here is the relative relationship between the axial flow velocity of the carry-over at the clearance and the peripheral flow velocity on the expansion groove wall. In the case of Ps=250Pa shown in Fig. 8, the axial flow velocity of the carry-over at the clearance is about 13~15m/s and the peripheral flow velocity on the expansion groove wall is higher than 15m/s. Thus, there is not a significant flow velocity difference between them. However, in the case of Ps=50Pa shown in Fig. 11, the axial flow velocity of the carry-over at the clearance is about 5~8m/s. And the peripheral flow velocity on the expansion groove wall is higher than 15m/s. In contrast to the statement above, there is a significant flow velocity difference between them. That is to say, the flow at the clearance is drawn into the expansion grooves by the viscosity of the peripheral flow on the walls that is about two or three times the velocity of that at the clearance. This phenomenon, which greatly changes the flow direction and then cuts off the carry-over in the axial direction, is a main cause of the decreases in the leakage rate. In the case of Ps=250Pa shown in Fig. 8, a small velocity difference between the axial flow velocity of the carry-over and the peripheral flow velocity on the groove wall did not lead to the separation of the carry-over flow from the shroud wall and its cut-off. Even though the separation of the carry-over flow may not result, it is thought that the carry-over flow is still drawn slightly toward the expansion grooves by the peripheral flow on the groove wall due to viscosity. Therefore, this phenomenon is also the reason for the leakage rate decrease in Fig. 8, even though that reason

was not revealed in chapter 4.2. Consequently, such a cut-off phenomenon of the carry-over arises, when the axial flow velocity of the carry-over at the clearance is smaller than the peripheral flow velocity on the expansion groove wall and the relative velocity of these two flows reaches a certain degree.

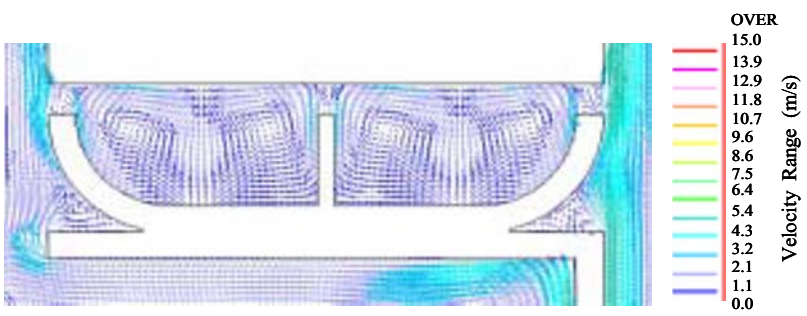

(a) Resultant velocity of the axial and radial components when the ring speed U=37.9m/s (R_ω=7.0×10^3)

(b) Contour map of peripheral velocity when the ring speed U=37.9m/s (R_ω=7.0×10^3)

Fig. 14. Visualization with CFD when the pressure condition Ps =0Pa (1-λ=0).

5. Conclusions

When the rotation is given to a labyrinth seal that operates in an extremely low static pressure difference and a large clearance, the leakage rate significantly decreases at low peripheral velocity. This differs from the results of the past research and its causes have been unknown. Therefore, the analyses of the internal flow within the labyrinth seal are conducted through CFD in order to reveal the reasons for the occurrence of this phenomenon.

The CFD computation results successfully show that the leakage rate greatly decreases due to the cut-off of the carry-over flow at the clearance when the ring is rotating. The carry-over flow is separated from the inner wall of the shroud and is drawn into the expansion grooves in curvature. This cut-off phenomenon of the carry-over arises due to viscous force that is caused by a relative velocity difference between the axial flow velocity of the carry-over and the much higher flow velocity in the peripheral direction on the wall of the expansion grooves. This high flow velocity in the peripheral direction occurs due to the viscous friction between the rotating labyrinth seal and the air. Such a phenomenon has never been pointed out as the reason for the decrease of the leakage rate by the rotation of the labyrinth seal.

Taking advantage of this phenomenon leads to the higher performance of a labyrinth seal with a large clearance, and thus large carry-over, when the operating static pressure difference is low. Therefore, it will be possible to apply this knowledge to a wider variety of uses.

Acknowledgments

The authors wish to express their gratitude to emeritus Dr. Koichi Ohyama (emeritus) of the National Aerospace Laboratory of Japan, who has given them many pieces of valuable advice in the design theory of the labyrinth seal.

References

Shimada, K., Kimura, K. and Watanabe, H., A Study of Radiator Cooling Fan with Labyrinth Seal, Trans. of JSAE, 20024053, 33-1 (2002), 63.

Shimada, K., Kimura, K., Ohta, H. and Aoki, K., Phenomenon of Labyrinth Seal with Small Operating Pressure and Large Clearance, Prediction of Performance and Experimental Result, Journal of Visualization, 6-4(2003), 395.

Komotori, K. and Miyake, K., Leakage Characteristics of Labyrinth Seals with High Rotating Speed, Proc. of 1977 Tokyo Joint Gas Turbine Congress, ASME-JSME-GTSJ, 45 (1977), 371.

Miyake,K. and Ariga,I., Leakage Characteristics of Rotating Stepped Labyrinth Seals, Trans. of JSME, (B), 51-466(1985), 1975.

Computational Dynamics Limited, Methodology STAR-CD Version 3.10A (1999).

Author Profile

Kota Shimada: He obtained his B.S. degree in mechanical engineering from Tokai University in 1992. He has worked for Toyo Radiator Co.,Ltd. as an engineer and has been engaged in the development of cooling fan systems for radiators since 1992. All japanese motorbike companies and some japanese automobiles companies currently use his fan design. His professional interests are focused on the design and analysis of axial flow fans which operate under unusual conditions.

Kazuhide Kimura: He received his B.S. degree in mechanical engineering from Ritsumeikan University in 1999. Since 1999, he has been working for Toyo Radiator Co.,Ltd.. He has been engaged in a design and analysis of cooling fans and radiators.

Susumu Ichikawa: He received his B.S. and M.S. degree in mechanical engineering in 1993 and 1995 from Musashi Institute of Technology. Since 1995, he has been working for Toyo Radiator Co.,Ltd.. His current research interests are analysis of internal flow and internal phenomenon of numerous different types of heat exchangers for fuel cell systems by using CFD.

Hiroaki Ohta: He received his B. Sc. (Eng.) and M. Sc. (Eng.) degree in mechanical engineering in 1970 and 1972 from Tokai University, and his Ph. Dr. in mechanical engineering in 2000 from the same University. After obtaining his M. Sc., he worked as a research assistant and a lecturer at Tokai University, before taking up his current position as an associate professor of Tokai University. His current research interests cover performance and flow inside impeller of centrifugal pump for high-viscosity liquids, performance of axial flow fans and flow around a half column.

Katsumi Aoki: He received his M.Sc.(Eng.) degree in mechanical engineering in 1967 from Tokai University, and his Ph.D. in mechanical engineering in 1986 from the same University. After obtaining his M.Sc., he worked as a research assistant, a lecturer, and an associate professor at Tokai University before taking up his current position as a professor of Tokai University. His current research interests cover flow around a rotating circular cylinder with and without grooves, flow around a rotating sphere, possibility of drag reduction using triangle-type cavity, and flow visualization by spark tracing method of complicated flow field as in centrifugal blower.